

A Diverse Population of $z \sim 2$ ULIRGs Revealed by JWST Imaging

J.-S. HUANG,^{1,2} ZI-JIAN LI,^{1,3} CHENG CHENG,¹ MEICUN HOU,⁴ HAOJING YAN,⁵ S. P. WILLNER,² Y.-S. DAI,¹
X. Z. ZHENG,^{6,7} J. PAN,^{1,8} D. RIGOPOULOU,^{9,10} T. WANG,^{11,12} ZHIYUAN LI,^{11,12} PIAORAN LIANG,^{1,3} A. ESAMIN,^{13,3} AND
G. G. FAZIO²

¹Chinese Academy of Sciences South America Center for Astronomy, National Astronomical Observatories, CAS, Beijing, 100101, China

²Center for Astrophysics | Harvard & Smithsonian, 60 Garden St., Cambridge, MA 02138 USA

³University of Chinese Academy of Sciences (UCAS), Beijing, 100049, China

⁴The Kavli Institute for Astronomy and Astrophysics, Peking University, Beijing, China

⁵Department of Physics and Astronomy, University of Missouri, Columbia, MO 65211, USA

⁶Purple Mountain Observatory, Chinese Academy of Sciences, 10 Yuanhua Road, Qixia District, Nanjing 210023, China

⁷School of Astronomy and Space Sciences, University of Science and Technology of China, Hefei 230026, China

⁸College of Earth Sciences, Guilin University of Technology, Guilin 541004, China

⁹Department of Astrophysics, Oxford University, Keble Road, Oxford, OX1 3RH, UK

¹⁰School of Sciences, European University Cyprus, Diogenes Street, Engomi, 1516 Nicosia, Cyprus

¹¹School of Astronomy and Space Science, Nanjing University, Nanjing 210046, China

¹²Key Laboratory of Modern Astronomy and Astrophysics (Nanjing University), Ministry of Education, Nanjing 210046, China

¹³Xinjiang Astronomical Observatory, Chinese Academy of Sciences, Urumqi, Xinjiang 830011, China

ABSTRACT

Four ultra-luminous infrared galaxies (ULIRGs) observed with JWST/NIRcam in the Cosmos Evolution Early Release Science program offer an unbiased preview of the $z \sim 2$ ULIRG population. The objects were originally selected at 24 μm and have strong polycyclic aromatic hydrocarbon emission features observed with Spitzer/IRS. The four objects have similar stellar masses of $\sim 10^{11} M_{\odot}$ but otherwise are quite diverse. One is an isolated disk galaxy, but it has an active nucleus as shown by X-ray observations and by a bright point-source nucleus. Two others are merging pairs with mass ratios of 6–7:1. One has active nuclei in both components, while the other has only one active nucleus: the one in the less-massive neighbor, not the ULIRG. The fourth object is clumpy and irregular and is probably a merger, but there is no sign of an active nucleus. The intrinsic spectral energy distributions for the four AGNs in these systems are typical of type-2 QSOs. This study is consistent with the idea that even if internal processes can produce large luminosities at $z \sim 2$, galaxy merging may still be necessary for the most luminous objects. The diversity of these four initial examples suggests that large samples will be needed to understand the $z \sim 2$ ULIRG population.

Keywords: Ultraluminous infrared galaxies Active galactic nuclei High-redshift galaxies Spectral energy distribution

1. INTRODUCTION

The global star-formation-rate density (GSFRD) of the Universe peaked about 10 Gyr ago, an epoch that corresponds to redshift $z \sim 2$. This era is often called “cosmic noon.” At any redshift, galaxies of higher mass tend to have higher star-formation rates (SFRs). This is known as the “star-formation main sequence.” Galax-

ies of all masses had higher SFR in the past, i.e., the star-formation main sequence has evolved to lower SFRs over time (Noeske et al. 2007; Speagle et al. 2014; Sandles et al. 2022). The $z \sim 2$ population with the highest SFRs, known as ultra-luminous infrared galaxies (ULIRGs), was the predominant contributor to the GSFRD at cosmic noon (Le Flocc’h et al. 2005; Caputi et al. 2007; Huang et al. 2009; Eser 2014). Though there are arguments that the SFR at the high-mass end of the star-formation main sequence might have been relatively constant rather than continuing to rise with mass (Whitaker et al. 2014; Leslie et al. 2020), ULIRGs at

$z \sim 2$ have stellar masses $M_* > 10^{11} M_\odot$ (Huang et al. 2009; Fang et al. 2014), and their descendants are today’s most massive galaxies.

The mechanism for triggering the prodigious SFRs characteristic of ULIRGs is unknown, but morphological studies can contribute to understanding it. Most local ULIRGs are major mergers (Sanders & Mirabel 1996; Bushouse et al. 2002; Kim et al. 2002; Sanders et al. 2003), but at higher redshifts, the morphological mix changes. Kartaltepe et al. (2012) studied 52 ULIRGs at $1 < z < 3$ in the GOODS survey areas and found that only 49% were mergers. In a study ten times larger in the COSMOS field, Ling & Yan (2022) found a morphological transition of ULIRG hosts at $z \approx 1.25$, above which merger galaxies dominate and below which disk and merger galaxies contribute similar fractions. At $z \approx 2$, mergers made up $\sim 50\%$ and disk galaxies $\sim 22\%$ of ULIRG hosts. Even if they were a minority, it appears that some galaxies at $z > 1$ were so gas-rich that they could become ULIRGs without merging. More recently, James Webb Space Telescope (JWST) observations that resolve sub-millimeter galaxies (SMGs) in the mid-infrared bands revealed that those qualifying as ULIRGs were all non-merging disk galaxies (Cheng et al. 2022, 2023).

Previous studies of high- z ULIRGs have suffered from two major disadvantages related to severe internal dust extinction. The first disadvantage is that ground-based spectroscopy to determine redshifts is expensive or even impossible because the dust extinction makes the galaxies so faint. Photometric redshifts remain an option for these galaxies, but the derived redshifts can depend on the amount of extinction (Huang et al. 2011), at least for IR-selected galaxies. This leads to large uncertainties in photometric redshifts. The other difficulty is the morphological K-correction (Taylor-Mager et al. 2007). Neither the stellar population nor the extinction has to be uniform, and therefore galaxies can show different morphologies in different bands. In rest-frame blue light, in particular, a non-uniform distribution of dust can drastically alter a galaxy’s morphological appearance, and any older stellar population will be faint. The longest-wavelength HST band is F160W, and at $z \geq 2$, this band samples rest-frame wavelengths shorter than 5000 \AA , where dusty or old stellar populations are faint or invisible.

This paper presents rest-frame near-infrared morphologies of four $z \sim 2$ ULIRGs based on JWST/NIRcam images. The JWST data come from the public Cosmic Evolution Early Release Science Survey (CEERS—Kocevski et al. 2022). The galaxies were identified as ULIRGs by a Spitzer/IRS survey

(Huang et al. 2009; Fang et al. 2014) and therefore have known redshifts. All four have strong polycyclic-aromatic-hydrocarbon (PAH) emission at rest $7.7 \mu\text{m}$ and high far-infrared luminosities. Three systems have X-ray detections with the Chandra X-ray Observatory and presumably contain AGNs. Previous studies have been limited to using spectral-energy-distribution (SED) modeling to separate AGNs and their host galaxies (Burgarella et al. 2005; Noll et al. 2009; Boquien et al. 2019; Huang et al. 2021). In contrast, the JWST angular resolution of $0''.07\text{--}0''.14$ ($=0.6\text{--}1.2 \text{ kpc}$ at $z = 2$)¹ in the NIRcam $2\text{--}4.4 \mu\text{m}$ bands can show a dusty AGN as a point source distinct from the galaxy disk. This allows us to derive physical parameters for AGNs and their host galaxies based on morphological separation of the components. Section 2 of this paper describes the sample selection, input data, and source SEDs. Section 3 discusses source morphologies, and Section 4 discusses the AGN components. Section 5 summarizes the results. All distances are based on a flat Λ CDM cosmology with $h = 0.7$, $\Omega_M = 0.272$, and $\Omega_\Lambda = 0.728$.

2. FULL SEDS OF $z \sim 2$ ULIRGS

Huang et al. (2009) and Fang et al. (2014) presented 20–38 μm Spitzer/IRS spectra of 24 μm -selected sources in the Extended Groth Strip (EGS). The selection criteria, involving $3.6\text{--}8.0 \mu\text{m}$ IRAC colors as well as 24 μm flux density were designed to select star-forming galaxies with strong PAH emission at $1.7 \lesssim z \lesssim 2.3$ (Huang et al. 2004, 2009). Nevertheless, some sample galaxies have an AGN component that produces mid-IR power-law emission (Huang et al. 2021). Most of the sample galaxies were also detected by Herschel in the far infrared, and some have been detected at submillimeter and millimeter wavelengths. All sources have a total infrared luminosity $>10^{12} L_\odot$. Only five sources from the two IRS samples are within the coverage of the CEERS images. One source, EGS 25, is actually at $z = 1.35$ (Momcheva et al. 2016) rather than $z = 1.65$, and we excluded it from this study.² The remaining four have redshifts based on strong PAH emission seen in the IRS spectra (Huang et al. 2009; Fang et al. 2014), and the PAH emission (along with the infrared luminosity) is another indicator of vigorous star formation. While this initial sample is small, it can be considered a random sample of the $z \approx 2$ ULIRG population with strong PAH emission.

¹ For all four systems, the scale is $8.4 \pm 0.1 \text{ kpc arcsec}^{-1}$.

² Fang et al. (2014) misidentified a strong [Ne II] line at $12.81 \mu\text{m}$ rest as the $11.3 \mu\text{m}$ PAH feature. The PAH feature may be present in the IRS spectrum but is weak.

Table 1. Measured data for the ULIRGs

Name	[SWM2014]	RA	Dec	$F(24\ \mu\text{m})$	z_{IRS}	$z_{3\text{D}}$	$\log_{10}(\frac{M_*}{M_{\odot}})$	A_V	$\log_{10}(\frac{L_{\text{IR}}}{L_{\odot}})$
	AEGIS	J2000		mJy					
EGS 11	23645	214.82267	52.82264	0.59	1.80±0.02	1.805	11.28±0.10	3.21±0.01	12.54
EGS 14	<i>a</i>	214.75113	52.83003	1.05	1.87±0.06	1.882	11.18±0.09	1.89±0.28	13.00
					stellar nucleus fit		11.41±0.20	2.67±0.01	
EGS 22	<i>b</i>	215.16037	52.96389	0.37	1.94±0.10	...	11.29±0.14	2.48±0.47	12.30
EGS 27 ^c	11754	214.89879	52.85250	0.49	2.29±0.09	2.372	10.95±0.12	1.58±0.29	12.56
					stellar nucleus fit		10.95±0.06	2.14±0.05	
EGS 14 blue ^d	...	214.750720	52.829797	10.55±0.10	1.11±0.13	...
					stellar nucleus fit		10.73±0.14	1.43±0.32	
EGS 14 red ^c	...	214.751102	52.830026	11.39±0.18	2.5±0.5	...
					stellar nucleus fit		11.49±0.15	2.49±0.45	
EGS 22 neighbor ^c	...	215.159845	52.963720	10.40±0.14	0.42±0.48	...
					stellar nucleus fit		11.02±0.95	1.37±0.54	

^ablend of 38174 and 38187

^bnot in 3D-HST area

^cX-ray source

^dAGN but not an X-ray source

NOTE—Sources above the line represent whole systems. Positions, 24 μm flux densities, and IRS redshifts are from Huang et al. (2009) for EGS 11/14 and Fang et al. (2014) for EGS 22/27. EGS 22 has a neighbor $1''.3$ away which contributes to $\lambda > 5.8\ \mu\text{m}$ photometry. Catalog identifications in column 2 are from Skelton et al. (2014), and 3D-HST redshifts in column 7 are from Momcheva et al. (2016). Sources below the line are from this paper. Positions refer to the bright, pointlike nuclei and are from the NIRCcam F277W images, which give the best combination of angular resolution and S/N for the nuclei. These pointlike sources are either AGNs or compact stellar bulges surrounding AGNs. There are two SED fits for each source, treating the nuclei as AGN or stellar bulges, respectively. Physical parameters were derived with CIGALE and are based on a Chabrier (2003) IMF, delayed exponential star formation history, and Calzetti et al. (2000) reddening law.

Images used here came from the CEERS image release v0.5 (Bagley et al. 2022)³ for three sources and from newer NIRCcam images for EGS 22. The new images were observed in 2022 December and are not included in CEERS image release v0.5. Therefore, for EGS 22, we utilized the MAST⁴ NIRCcam stage 3 mosaic calibrated by pipeline v1.8.2 with pmap version `jwst_1030.pmap`.

Figure 1 shows the resulting NIRCcam images of the four sources along with existing HST images, and Table 1 gives the galaxies’ properties. All four have red colors and show multiple nuclei with surrounding extended structure. The most complex source is EGS 14, which has two components with differing colors. Much of the

southwestern (“blue”) component is seen in the HST F606W (not shown) and F814W images, but the northeastern (“red”) component has only a trace detected in F814W and is invisible in F606W. Both components show a bright, pointlike nucleus. Neither nucleus is seen in F606W, and they are faint in F814W. EGS 22 shows two objects in the NIRCcam images, $1''.3$ apart (Figure 1). The northeastern galaxy shows spiral arms with some clumps visible in the short-wave JWST images. A red, pointlike nucleus is visible in F277W and longer bands. The southwestern galaxy shows an extended disk around a bright, pointlike nucleus. The MIPS 24 μm detection is close to the northeastern galaxy, but both may contribute to the detected MIPS 24 μm flux. EGS 22 is outside the 3D-HST coverage, so there is no other spectroscopic redshift. The IRS spectrum (Fang et al. 2014) shows only one redshift system. Photometric redshifts are 1.83 and 1.70 for the two sources, close to the IRS redshift. EGS 22 is therefore likely to be a real galaxy pair in the process of merging, as also suggested by a

³ <https://ceers.github.io/dr05.html#nircam-imaging>

⁴ <https://mast.stsci.edu/portal/Mashup/Clients/Mast/Portal.html>

slight distortion of the northeastern galaxy’s spiral arms. EGS 11 and EGS 27 are barely detected in the F606W and F814W HST bands but obvious in the HST 1.6 μm and all JWST images. EGS 27 has one bright, pointlike nucleus seen most prominently in the reddest JWST bands and invisible in F814W. This nucleus is offset by ~ 1.4 kpc (in projection) from the centroid of the clumpy galaxy disk. EGS 11 has three or more pointlike components, but none of them is as bright as the nuclei seen in the other two sources.

We performed elliptical-aperture photometry with radii matching the 3σ surface-brightness contour for each object. For EGS 14 and EGS 22, the extended components are well separated from the two nuclei in the F115W and F150W images, and we measured flux densities for the two components separately. The multiple nuclei in EGS 11 show that it is also a merging system, but we treated it as a single galaxy because the components are too close to separate. We also measured flux densities for the point sources in EGS 14 and EGS 27 with $0''.09$ apertures corrected to total magnitudes using the point-spread function in each band.

We derived physical parameters for each source by fitting their SEDs with CIGALE (Burgarella et al. 2005). Typically CIGALE uses three components—stellar emission, an AGN, and a dusty star-forming component in the infrared bands—to fit the full SED of a galaxy. The fit yields the percentage of each component’s contribution to the total SED. One advantage of SED fitting using JWST images is that we can morphologically separate components, in particular the pointlike components in EGS 14/22/27. We fitted those in two ways. One was to treat the nucleus as an AGN, fit it separately, subtract its light, and then fit the extended component with only stellar emission (and dust extinction). The other fit treated the nucleus as a stellar bulge and included it as part of the stellar population. Whether the pointlike sources are treated as AGNs or stellar bulges does not significantly change the total stellar masses. We fitted the blue and red components of EGS 14 separately to determine their dust extinctions and to obtain the intrinsic SEDs for the pointlike sources in both components. EGS 11 has no bright, pointlike component, no X-ray detection, and its 15-to-24 μm flux density ratio is inconsistent with an AGN (Huang et al. 2009). If an AGN is present, it isn’t contributing to the observed NIRCcam fluxes. We therefore fit its SED with only stellar and dust components. The SEDs and fits are shown in Figure 2, and the derived physical parameters are in Table 1. All galaxies in the four systems have stellar mass $M_* \sim 10^{11} M_\odot$. Fitting the FIR and submillimeter confirms that all systems contain ULIRGs

with EGS 14 close to being a HyperLIRG, but the Herschel angular resolution cannot separate the individual galaxies in each system.

3. JWST MORPHOLOGY OF $z \sim 2$ ULIRGS

EGS 11, 14, and 22 are merging systems as shown by both HST/WFC3 and JWST/NIRcam images. Each source shows only a single redshift system in Spitzer/IRS and HST/3D spectra (within the uncertainties), further evidence that the components are at least associated. EGS 11 has a clumpy structure with at least a dozen clumps visible in the F150W image. Fewer clumps are visible at longer wavelengths because the angular resolution is worse. EGS 14 has morphology similar to a familiar merging system, the Antennae, with one component luminous in the rest ultraviolet and the other luminous in the rest near-infrared. The projected distance between the two point-source nuclei is $1''.17 = 9.8$ kpc, similar to the 7 kpc separation between the Antennae galaxies. High-redshift, merging ULIRGs resolved with ALMA have typical projected separations of 7–8 kpc (Rujopakarn et al. 2016; Hodge et al. 2016; Gómez-Guijarro et al. 2018; Rujopakarn et al. 2019), and EGS 14 looks to be another member of this class. EGS 22 is also a merging system with a projected separation of 10.9 kpc, larger than those for EGS 11 and 14. It appears to be in an early stage of merging.

In contrast to the other systems, EGS 27 is an isolated galaxy in the JWST NIRcam bands. GALFIT confirmed that its morphology in the F444W band is a disk with Sérsic index $n = 0.7$ and effective radius $r_e = 5$ kpc. This is slightly larger than SMGs in SMACS 0723 (Cheng et al. 2022) and distinctly larger than r_e of the fainter SMG population (Cheng et al. 2023). However, absence of interaction doesn’t mean low SFR: EGS 27, despite being an isolated disk, has $\log(L_{\text{IR}}/L_\odot) \sim 12.5$, comparable to the two merging sources.

Despite EGS 14’s similar appearance to the Antennae, it has $100\times$ higher infrared luminosity than that system (Sanders et al. 2003; Seillé et al. 2022). Its normalized SFR, $\log(\text{SFR}/\text{SFR}_{\text{MS}})$, is 0.92, $\gg 0.3$ dex above the star-formation main-sequence at $1.5 < z < 2$ (Whitaker et al. 2014), putting this galaxy into the starburst regime (Hogan et al. 2021). The normalized SFRs for EGS 11 and EGS 27 are 0.40 and 0.48, respectively, just above the main-sequence upper limit. The normalized SFR for EGS 22, using the sum of the two masses, is 0.15. If all the FIR luminosity comes from the northeastern galaxy, the normalized SFR would be 0.21. These normalized SFRs are high but not significantly above the main sequence.

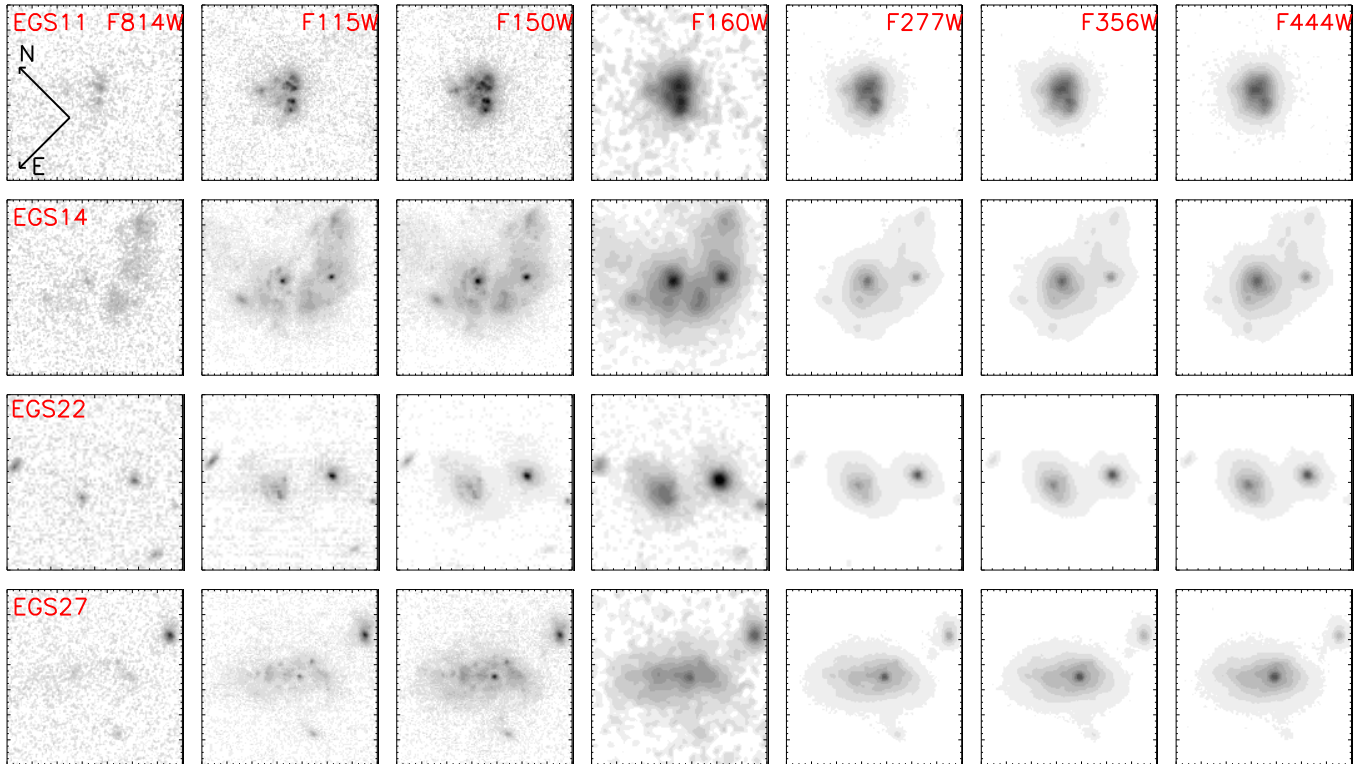


Figure 1. Negative stamp images of the four sources. Each panel is $4''2$ in size. Sources are labeled in the left panel of each row. All images have almost the same orientation as shown in the top-left panel. Images in the leftmost column are HST F814W and in the fourth column HST F160W. Other images are from JWST/NIRCam as labeled in the top row. With only HST images, EGS 14 would be identified as a major merger because the two components have very similar magnitudes in the HST F160W band.

At high redshift, merging is more likely in higher-luminosity systems. An ALMA sample at $z \sim 4.5$ with $\log(L_{\text{IR}}/L_{\odot}) \geq 12.65$ (Gómez-Guijarro et al. 2018) found that six of seven systems studied, including all three HyperLIRGs, are minor mergers.⁵ Evidently even a minor merger of two gas-rich galaxies can induce a ULIRG at high redshifts. EGS 11/14 have merging morphologies similar to those of the ALMA sample. The mass ratio for EGS 14 is ~ 7 , and the mass ratio range for the Gómez-Guijarro et al. (2018) sample at $z \sim 4.5$ is $3 < M_1/M_2 < 16$ with only two systems having mass ratios < 4 . EGS 22 has a mass ratio ~ 6 , but it has a larger distance between galaxies than the others, and the system is not in a starburst stage. The existing data suggest that a minor merger between two or more gas-rich galaxies can trigger luminosities $> 10^{13} L_{\odot}$.

4. IDENTIFYING AGNS IN $z \sim 2$ ULIRGS

The two bright, pointlike nuclei in EGS 14, the one in the EGS 22 neighbor, and the one in EGS 27 are unre-

solved in the F115W images. (The nucleus of EGS 22 itself is too red to be visible in F115W.) This implies sizes smaller than $0''.1$ or 800 pc. The small size suggests the nuclei are AGNs, but based on size alone, they could be compact stellar or gaseous structures. Stronger evidence is that EGS 14/22/27 were detected by Chandra in 800 ks exposure time. (They are among 25% of the original PAH-selected samples that have Chandra detections—Huang et al. 2009; Fang et al. 2014.) In contrast, EGS 11 has no X-ray detection and shows no point source as bright as the ones in EGS 14/22/27. The EGS 14 Chandra image shows only one detection at position (214.75116, 52.830010), $0''.3$ from the red component and $1''.4$ from the blue component of that system. The red component is 1.6 magnitudes brighter in the F444W band (rest $1.5 \mu\text{m}$) than the blue component (Figure 2). Based on both position and near-IR luminosity, the red component is therefore likely to be the dominant contributor to the X-ray flux. The EGS 22 Chandra image also has one detection at position (215.15999, 52.963689).⁶ This is $1''.4$ from the

⁵ A major merger requires mass ratio $M_1/M_2 < 4$ —Man et al. 2016.

⁶ <https://cxc.cfa.harvard.edu/csc/>

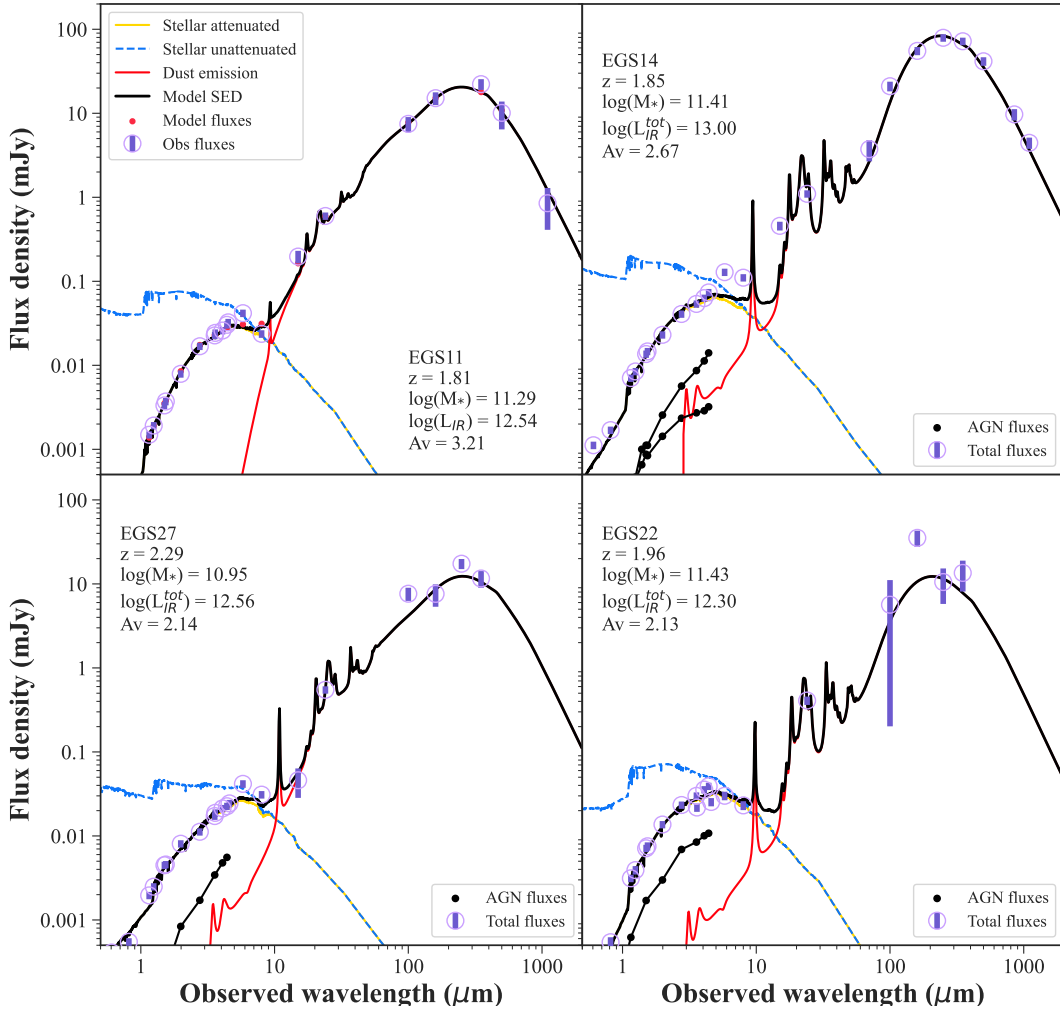


Figure 2. SED fits using CIGALE. Open circles with error bars show the measured flux densities. For EGS 14/22, these are for both components because they cannot be separated at wavelengths beyond $5 \mu\text{m}$. Plain lines show the model flux densities as indicated in the legend at top left, and lines with filled circles show the separate AGN fits. Legends in each panel give fit parameters, which include both components for EGS 14/22. The Herschel photometry data are from [Lutz et al. \(2011\)](#) and [Oliver et al. \(2012\)](#), and the submillimeter and millimeter photometry data are from [Zavala et al. \(2017\)](#) and [Younger et al. \(2009\)](#). The only available constraint on AGN models at wavelength $>4.44 \mu\text{m}$ is that they should not exceed the observed total flux densities.

EGS 22 northeastern galaxy and $0''.13$ from its southwestern neighbor, which must be the X-ray source. This identification is consistent with this galaxy’s bright, pointlike nucleus. The EGS 27 X-ray emission is unambiguously from the NIRCcam point source with an offset between positions of $0''.24$, well within the Chandra position uncertainty. The X-ray luminosities, $L(0.5\text{--}8 \text{ keV})$, of EGS 14/22/27, even with no correction for H I absorption, are $1.1 \times 10^{43} \text{ erg s}^{-1}$, $1.9 \times 10^{43} \text{ erg s}^{-1}$, and $4.5 \times 10^{43} \text{ erg s}^{-1}$, respectively, well into the AGN range.

EGS 14 has a very different X-ray SED than EGS 22/27 have. EGS 14’s hardness ratio⁷ is 0.32. This implies that it is obscured with a column density possibly larger than 10^{22} cm^{-2} . EGS 22/27 have similar hardness ratios of -0.29 , below the traditional obscured-AGN limit of -0.2 . At high redshift, HR is less affected by a given column density, and at $z = 1.94$ and 2.31 , H I column densities can be as high as 10^{22} cm^{-2} according to X-ray hardness models ([Hasinger 2008](#); [Elvis et al. 2012](#)). In any case, EGS 14 has a column density

⁷ $\text{HR} \equiv [(H - S)/(H + S)]$, where H and S are hard (2–8 keV) and soft (0.5–2 keV) counts, respectively.

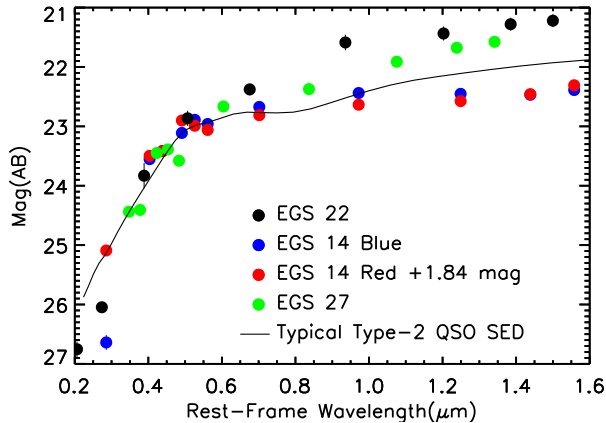


Figure 3. SEDs of the four AGN sources identified in Table 1. Points show photometry for these sources indicated by color as shown in the legend. The EGS 14 red source is offset (plotted fainter) to allow better comparison with the others. All photometry has been corrected for the host-galaxy dust extinction. The solid line is a typical type-2 QSO template (Hickox et al. 2017) for comparison. All four SEDs show a similar 4000 Å break, as does the template.

an order of magnitude higher than the other two X-ray sources, but all the visible–NIR SEDs have a similar shape as shown in Figure 3. The host galaxies for the three X-ray sources have dust extinctions in line with the X-ray obscuration with $A_V = 2.5$ for the EGS 14 X-ray counterpart versus $A_V = 0.4$ for the EGS 22 neighbor and $A_V = 1.6$ for EGS 27. (These extinctions are for the host galaxies after subtracting the point sources, as appropriate if the point sources are AGNs.) The blue point-source in EGS 14 has low dust extinction in its host galaxy, but despite that, no X-ray source was detected. After correction for host-galaxy extinction, all four point sources have similar SEDs, as shown in Figure 3, with all four SEDs showing a steep decrease at $\lambda_{\text{rest}} \lesssim 0.4 \mu\text{m}$. A downturn like this is often seen in type-2 QSO SEDs dominated by an old stellar population in the bulge around a central AGN (Hickox et al. 2017). The match between the observed SEDs and the type 2 AGN template further confirms that all four point sources are type-2 AGNs. If we ignore the evidence for AGNs and pretend the pointlike sources are stellar, upper limits for their masses are ~ 1.8 , 6.3, 13.3, and $4.0 \times 10^{10} M_\odot$ for the EGS 14 blue, red, EGS 22 neighbor, and EGS 27 sources, respectively.

5. SUMMARY

Four luminous objects initially selected as Spitzer 24 μm sources have now been observed by JWST/NIRCam. Redshifts ($1.8 \leq z \leq 2.3$) are known from Spitzer/IRS spectra, and luminosities

$L_{\text{IR}} > 10^{12.3} L_\odot$ for all systems. All four objects are so red that they are barely detected by HST at wavelengths $< 1 \mu\text{m}$. The NIRcam images permit morphological studies and measurement of SEDs for each component. One of the four objects is a clumpy disk, probably a merger, with no sign of an AGN. A second object is a minor-merger system (mass ratio 7:1) with two AGNs. Evidently even a mass ratio this large can trigger a near-HyperLIRG at $z = 1.87$. The third object is also a likely merger with a neighbor $1''.3$ away. The neighbor hosts an AGN. The merger is likely in an early stage, and its mass ratio is 6:1. The fourth object is an isolated disk galaxy with an AGN. Its effective radius is ~ 5 kpc, about as large as the Milky Way. All four systems have stellar masses near $10^{11} M_\odot$. The AGN contributions to the broad-band photometry are less than 25% and do not significantly change the stellar mass estimates.

None of the four point sources identified as an AGN was obvious in the HST ACS F606W and F814W images. In contrast, those objects are easy detections at 2.8 μm and longer wavelengths. After correction for host-galaxy dust extinction, the four AGNs have SED shapes similar to a typical type-2 QSO. Three of the four AGNs were detected in X-rays by Chandra, but the less-obscured AGN in the EGS 14 merging system was not. The X-ray spectral analysis confirms the AGN nature of the sources and shows high H I column density for one of them.

The observations give an intriguing first look at the most luminous star-forming galaxies at $z \approx 2$. If the wide diversity in these first four examples is typical of the population, very large samples will be needed to understand the ULIRG population at cosmic noon.

This work was sponsored by the National Key R&D Program of China grant No. 2022YFA1605300, the National Natural Science Foundation of China (NSFC) grants No. 11933003, 12273051, and 11803044, and in part by the Chinese Academy of Sciences (CAS) through a grant to the CAS South America Center for Astronomy (CAS-SACA). This work is based on observations made with the NASA/ESA/CSA James Webb Space Telescope. Data presented in this paper were obtained from the Mikulski Archive for Space Telescopes at the Space Telescope Science Institute, which is operated by the Association of Universities for Research in Astronomy, Inc., under NASA contract NAS 5-03127 for JWST. These observations are associated with JWST program 1345. The JWST observations used here can be accessed via <https://doi.org/10.17909/vdav-5d38>. This research has made use of data obtained from the Chandra Source Catalog, provided by the Chandra X-ray Center (CXC) as part of the Chandra Data Archive.

Facilities: AKARI, Herschel(PACS, SPIRE), HST(ACS, WFC3-IR), Spitzer(IRAC, MIPS, IRS), JWST(NIRcam), CXO

REFERENCES

- Bagley, M. B., Finkelstein, S. L., Koekemoer, A. M., et al. 2022, arXiv e-prints, arXiv:2211.02495.
<https://arxiv.org/abs/2211.02495>
- Boquien, M., Burgarella, D., Roehlly, Y., et al. 2019, *A&A*, 622, A103, doi: [10.1051/0004-6361/201834156](https://doi.org/10.1051/0004-6361/201834156)
- Burgarella, D., Buat, V., & Iglesias-Páramo, J. 2005, *MNRAS*, 360, 1413,
 doi: [10.1111/j.1365-2966.2005.09131.x](https://doi.org/10.1111/j.1365-2966.2005.09131.x)
- Bushouse, H. A., Borne, K. D., Colina, L., et al. 2002, *ApJS*, 138, 1, doi: [10.1086/324019](https://doi.org/10.1086/324019)
- Calzetti, D., Armus, L., Bohlin, R. C., et al. 2000, *ApJ*, 533, 682, doi: [10.1086/308692](https://doi.org/10.1086/308692)
- Caputi, K. I., Lagache, G., Yan, L., et al. 2007, *ApJ*, 660, 97, doi: [10.1086/512667](https://doi.org/10.1086/512667)
- Chabrier, G. 2003, *PASP*, 115, 763, doi: [10.1086/376392](https://doi.org/10.1086/376392)
- Cheng, C., Yan, H., Huang, J.-S., et al. 2022, *ApJL*, 936, L19, doi: [10.3847/2041-8213/ac8d08](https://doi.org/10.3847/2041-8213/ac8d08)
- Cheng, C., Huang, J.-S., Smail, I., et al. 2023, *ApJL*, 942, L19, doi: [10.3847/2041-8213/aca9d0](https://doi.org/10.3847/2041-8213/aca9d0)
- Elvis, M., Hao, H., Civano, F., et al. 2012, *ApJ*, 759, 6,
 doi: [10.1088/0004-637X/759/1/6](https://doi.org/10.1088/0004-637X/759/1/6)
- Eser, E. K. 2014, PhD thesis, University of Copenhagen, Denmark
- Fang, G., Huang, J.-S., Willner, S. P., et al. 2014, *ApJ*, 781, 63, doi: [10.1088/0004-637X/781/2/63](https://doi.org/10.1088/0004-637X/781/2/63)
- Gómez-Guijarro, C., Toft, S., Karim, A., et al. 2018, *ApJ*, 856, 121, doi: [10.3847/1538-4357/aab206](https://doi.org/10.3847/1538-4357/aab206)
- Hasinger, G. 2008, *A&A*, 490, 905,
 doi: [10.1051/0004-6361:200809839](https://doi.org/10.1051/0004-6361:200809839)
- Hickox, R. C., Myers, A. D., Greene, J. E., et al. 2017, *ApJ*, 849, 53, doi: [10.3847/1538-4357/aa8c77](https://doi.org/10.3847/1538-4357/aa8c77)
- Hodge, J. A., Swinbank, A. M., Simpson, J. M., et al. 2016, *ApJ*, 833, 103, doi: [10.3847/1538-4357/833/1/103](https://doi.org/10.3847/1538-4357/833/1/103)
- Hogan, L., Rigopoulou, D., Magdis, G. E., et al. 2021, *MNRAS*, 503, 5329, doi: [10.1093/mnras/stab527](https://doi.org/10.1093/mnras/stab527)
- Huang, J. S., Zheng, X. Z., Rigopoulou, D., et al. 2011, *ApJL*, 742, L13, doi: [10.1088/2041-8205/742/1/L13](https://doi.org/10.1088/2041-8205/742/1/L13)
- Huang, J. S., Barmby, P., Fazio, G. G., et al. 2004, *ApJS*, 154, 44, doi: [10.1086/422882](https://doi.org/10.1086/422882)
- Huang, J. S., Faber, S. M., Daddi, E., et al. 2009, *ApJ*, 700, 183, doi: [10.1088/0004-637X/700/1/183](https://doi.org/10.1088/0004-637X/700/1/183)
- Huang, J. S., Dai, Y. S., Willner, S. P., et al. 2021, *ApJ*, 912, 161, doi: [10.3847/1538-4357/abec50](https://doi.org/10.3847/1538-4357/abec50)
- Kartaltepe, J. S., Dickinson, M., Alexander, D. M., et al. 2012, *ApJ*, 757, 23, doi: [10.1088/0004-637X/757/1/23](https://doi.org/10.1088/0004-637X/757/1/23)
- Kim, D. C., Veilleux, S., & Sanders, D. B. 2002, *ApJS*, 143, 277, doi: [10.1086/343843](https://doi.org/10.1086/343843)
- Kocevski, D. D., Barro, G., McGrath, E. J., et al. 2022, arXiv e-prints, arXiv:2208.14480.
<https://arxiv.org/abs/2208.14480>
- Le Flo'ch, E., Papovich, C., Dole, H., et al. 2005, *ApJ*, 632, 169, doi: [10.1086/432789](https://doi.org/10.1086/432789)
- Leslie, S. K., Schinnerer, E., Liu, D., et al. 2020, *ApJ*, 899, 58, doi: [10.3847/1538-4357/aba044](https://doi.org/10.3847/1538-4357/aba044)
- Ling, C., & Yan, H. 2022, *ApJ*, 929, 40,
 doi: [10.3847/1538-4357/ac57c1](https://doi.org/10.3847/1538-4357/ac57c1)
- Lutz, D., Poglitsch, A., Altieri, B., et al. 2011, *A&A*, 532, A90, doi: [10.1051/0004-6361/201117107](https://doi.org/10.1051/0004-6361/201117107)
- Man, A. W. S., Zirm, A. W., & Toft, S. 2016, *ApJ*, 830, 89,
 doi: [10.3847/0004-637X/830/2/89](https://doi.org/10.3847/0004-637X/830/2/89)
- Momcheva, I. G., Brammer, G. B., van Dokkum, P. G., et al. 2016, *ApJS*, 225, 27,
 doi: [10.3847/0067-0049/225/2/27](https://doi.org/10.3847/0067-0049/225/2/27)
- Noeske, K. G., Weiner, B. J., Faber, S. M., et al. 2007, *ApJL*, 660, L43, doi: [10.1086/517926](https://doi.org/10.1086/517926)
- Noll, S., Burgarella, D., Giovannoli, E., et al. 2009, *A&A*, 507, 1793, doi: [10.1051/0004-6361/200912497](https://doi.org/10.1051/0004-6361/200912497)
- Oliver, S. J., Bock, J., Altieri, B., et al. 2012, *MNRAS*, 424, 1614, doi: [10.1111/j.1365-2966.2012.20912.x](https://doi.org/10.1111/j.1365-2966.2012.20912.x)
- Rujopakarn, W., Dunlop, J. S., Rieke, G. H., et al. 2016, *ApJ*, 833, 12, doi: [10.3847/0004-637X/833/1/12](https://doi.org/10.3847/0004-637X/833/1/12)
- Rujopakarn, W., Daddi, E., Rieke, G. H., et al. 2019, *ApJ*, 882, 107, doi: [10.3847/1538-4357/ab3791](https://doi.org/10.3847/1538-4357/ab3791)
- Sanders, D. B., Mazzarella, J. M., Kim, D. C., Surace, J. A., & Soifer, B. T. 2003, *AJ*, 126, 1607,
 doi: [10.1086/376841](https://doi.org/10.1086/376841)
- Sanders, D. B., & Mirabel, I. F. 1996, *ARA&A*, 34, 749,
 doi: [10.1146/annurev.astro.34.1.749](https://doi.org/10.1146/annurev.astro.34.1.749)
- Sandles, L., Curtis-Lake, E., Charlot, S., Chevallard, J., & Maiolino, R. 2022, *MNRAS*, 515, 2951,
 doi: [10.1093/mnras/stac1999](https://doi.org/10.1093/mnras/stac1999)
- Seillé, L. M., Buat, V., Haddad, W., et al. 2022, *A&A*, 665, A137, doi: [10.1051/0004-6361/202243702](https://doi.org/10.1051/0004-6361/202243702)
- Skelton, R. E., Whitaker, K. E., Momcheva, I. G., et al. 2014, *ApJS*, 214, 24, doi: [10.1088/0067-0049/214/2/24](https://doi.org/10.1088/0067-0049/214/2/24)
- Speagle, J. S., Steinhardt, C. L., Capak, P. L., & Silverman, J. D. 2014, *ApJS*, 214, 15,
 doi: [10.1088/0067-0049/214/2/15](https://doi.org/10.1088/0067-0049/214/2/15)
- Taylor-Mager, V. A., Conselice, C. J., Windhorst, R. A., & Jansen, R. A. 2007, *ApJ*, 659, 162, doi: [10.1086/511806](https://doi.org/10.1086/511806)
- Whitaker, K. E., Franx, M., Leja, J., et al. 2014, *ApJ*, 795, 104, doi: [10.1088/0004-637X/795/2/104](https://doi.org/10.1088/0004-637X/795/2/104)
- Younger, J. D., Omont, A., Fiolet, N., et al. 2009, *MNRAS*, 394, 1685, doi: [10.1111/j.1365-2966.2009.14455.x](https://doi.org/10.1111/j.1365-2966.2009.14455.x)
- Zavala, J. A., Aretxaga, I., Geach, J. E., et al. 2017, *MNRAS*, 464, 3369, doi: [10.1093/mnras/stw2630](https://doi.org/10.1093/mnras/stw2630)